Cold Regions Science and Technology 207 (2023) 103775

Contents lists available at ScienceDirect

Cold Regions Science and Technology

journal homepage: www.elsevier.com/locate/coldregions

A flight-testing campaign to examine inflight icing characteristics and its effects on the flight performance of an Unmanned-Aerial-Vehicle

Nianhong Han, M.A. Siddique, Zichen Zhang, Linchuan Tian, Haiyang Hu, Hui Hu *

Dept. of Aerospace Engineering, Iowa State University, Ames, IA 50011, USA

ARTICLE INFO

Keywords:
UAV flight testing
UAV aerodynamics
UAV icing
Propeller Icing
Icing-induced performance degradation

ABSTRACT

A flight-testing campaign was conducted to examine in-flight icing characteristics and its effects on the flight performance of a fixed-wing Unmanned-Aerial-Vehicle (UAV). While the UAV was deployed to fly autonomously along a pre-planned flight trajectory under a realistic, atmospheric icing condition, a suite of avionics/sensors was installed onboard to monitor both UAV flight parameters (e.g., UAV flying speed, flight altitude, and power consumption) and the environmental conditions (e.g., airspeed, ambient temperature, and relative humidity) along the flying path. Substantial ice structures were observed to accumulate on nearly all exposed airframe surfaces (e.g., wings, fuselage, stabilizers, Pitot probe and propeller) as the UAV finished the flight mission with evident inflight icing. While the ice accretion on the UAV wings and stabilizers were found to degrade their aerodynamic performances by decreasing lift while increasing drag, the ice layer accreted on the Pitot probe blocked the pressure holes, leading to false airspeed readings from the iced Pitot probe. The ice accretion on the rotating UAV propeller blades was found to degrade the propeller perfomance dramatically, resulting in over 80% more power consumption for the UAV to finish the same flight mission, in comparison to that under a non-icing condition. Inflight icing was also found to provoke significant structural vibrations, causing great challenges to UAV flight stability and imposing serious threats to the flight safety.

1. Introduction

Unmanned Aerial Vehicles, or UAVs in short, represent one of the most significant breakthroughs in the aerospace community. Since UAVs can be controlled remotely or sometimes autonomously, they have been widely used for various applications, including agriculture, urban planning, cargo transport, wildlife conservation, healthcare, and search and rescue (Aggarwal et al., 2017; Eckerstorfer et al., 2016; Pajares, 2015; Revuelto et al., 2021; Tsouros et al., 2019). In comparison to traditional manned aircraft, the cost and mortality reductions associated with deploying UAVs are also very appealing for military reconnaissance and surveillance. As a result, a collection of UAVs, such as Predator, Phoenix, and Global Hawk, have been used for achieving widespread military missions. With the fast expanding UAV applications, the effects of adverse weathers (e.g., raining, snowing and icing) on UAV flight performance need to be examined carefully for safe and efficient UAV operations under such adverse weather conditions (Bie et al., 2021; Hawley and Millstein, 2019; Hu et al., 2021).

Inflight icing is one of the most well-known aviation dangers that threats both unmanned and manned airplanes flying in cold climates (Cao et al., 2018; Ignatyev et al., 2020; Vercillo et al., 2019). Compared with large-sized, manned aircraft, small-sized UAVs are much more susceptible to inflight icing problems due to the lower cruising altitude associated with relatively warmer ambient temperatures and higher liquid water content (LWC) in the air, the slower flying speed to cause longer exposure time to icing conditions, and greater vulnerability to the damages of the electric sensors on-board (Hann and Johansen, 2021; Szilder and McIlwain, 2012). The possible damage caused by inflight icing tends to render UAV operation unfeasible in cold weather. The commonly-used UAV icing avoidance strategies are either to keep UAVs on the ground or to modify their flight paths, which would greatly reduce UAV operational capability in cold climates (Zhang et al., 2014).

Advancing the technology for safer and more efficient operation of UAVs in cold climates requires the development of novel and effective ice detection and anti−/de-icing strategies tailored specifically for UAV icing protection. Doing so requires a keen understanding of the underlying physics pertinent to UAV icing phenomena. Ice accretion on an airframe surface are usually categorized as *rime*, *glaze,* or *mixed ice*,

* Corresponding author.
E-mail address: huhui@iastate.edu (H. Hu).

https://doi.org/10.1016/j.coldregions.2023.103775
Received 22 July 2022; Received in revised form 5 December 2022; Accepted 9 January 2023
Available online 13 January 2023
0165-232X/

depending on the conditions under which the icing event occurs (Liu and Hu, 2018; Politovich, 2000). When the ambient temperature is relatively low (i.e., typically below −8.0 °C) and the incoming airflow is relatively dry (i.e., having a lower *LWC* value), supercooled water droplets carried by the incoming airflow would freeze immediately upon impacting onto the airframe surface, forming *rime* ice (Liu and Hu, 2018). At relatively warm temperatures just below the water freezing temperature (i.e., typically above −8.0 °C) with relatively high *LWC* levels in the incoming airflow, the impinged supercooled water droplets would be frozen only partially with the remaining impacted water mass running back along the ice accreting surface. The runback water would be frozen into ice subsequently at further downstream locations, forming *glaze ice* with much more complex ice shapes (Waldman and Hu, 2016). *Mixed icing* refers the situation with simultaneous appearance of both *rime* and *glaze* icing characteristics (Gao et al., 2019a).

A number of theoretic analysis and numerical studies have been conducted in recent years to evaluate the adverse effects of inflight icing on UAV operation capabilities (Hann et al., 2017; Hann and Johansen, 2021; Hann and Johansen, 2020; Karpen et al., 2022; Li et al., 2019; Liu et al., 2019; Müller and Hann, 2022; Oo et al., 2020; Oswald et al., 2022; Szilder and McIlwain, 2012; Szilder and Yuan, 2017; Winter et al., 2019). For example, Siquig (1990) conducted a theoretical analysis to evaluate the effects of ice accretion on UAV operation by comparing two different types of UAVs (i.e., high-flying, long-endurance UAVs vs. low-flying, short-endurance UAVs) flying under atmospheric icing conditions. Bottyán (2014) developed an inflight icing estimation method with a simple ice accretion model to examine the effects of airflow temperature, LWC level, airfoil geometry, and airflow speed on the ice accretion on UAV wings. Szilder and McIlwain (2012) conducted a numerical study to evaluate the effects of Reynolds number on the icing process for UAV applications. Hann et al. (2017) conducted a numerical study to evaluate the impact of ice accretion on aerodynamic lift and drag of an airfoil model for UAV applications.

Several experimental studies have also been conducted recently to characterize the detrimental effects of ice accretion on UAV aerodynamic performance. Liu et al. (2018b) conducted an icing tunnel testing campaign to examine the ice accretion characteristics over the blade surfaces of a rotating UAV propeller. Hann et al. (2020) performed an experimental study in Cranfield icing wind tunnel to characterize the ice accretion on the surface of a S826 airfoil model at low Reynolds number levels relevant to UAV flight. Yan et al. (2020) reported an experimental study to investigate a coaxial rotor system in an icing testing chamber in order to develop an empirical model to predict the changes in torque and thrust of the rotor pertinent to UAV icing scenario. Liu et al. (2019) characterized the icing-induced performance degradation of an UAV propeller based on the variations of the measured thrust force, power consumption and "phase-locked" flow filed measurements under different icing conditions. Liu et al. (2019) reported an experimental study to evaluate the influences of airframe thermal conductivity on the ice accretion pertinent to UAV icing phenomena. Research efforts have also been made to develop anti−/de-icing strategies for UAV icing mitigation. For example, Liu et al. (2018a) and Han et al. (2022a) demonstrate the feasibility of using hydro−/ice-phobic coatings to suppress the dynamic ice accretion on an UAV propeller. Armanini et al. (2016) and Sørensen et al. (2015) proposed to integrate a power control system and an electrically-conductive carbon-nano-material-based coating for UAV icing mitigation. Hann (2019) also reported a comparative study to explore the capability of two numerical icing codes, i.e., FENSAP-ICE and LEWICE, to assist the design of a UAV anti-icing protection system. More recently, Karpen et al. (2022) demonstrated the feasibility of a propeller-integrated airfoil heater system for small multirotor drones flying in icing environments.

While important findings about UAV icing and anti−/de-icing have been derived from the studies, almost all the previous studies were performed by conducting either numerical simulations with simplified assumptions or icing tunnel experiments with idealized laboratory settings. For example, UAVs were usually assumed to be exposed to uniform incoming airflows under idealized icing conditions, while staying in the same operational status during the entire ice accretion process. However, in reality, UAVs always fly in atmospheric boundary layer (ABL) airflows with constantly varying wind speed and directions (i.e., exposed to highly turbulent ABL winds with substantial gusts), let alone the complex weather changes (e.g., ambient temperature and LWC level changes) during icing events. There are knowledge gaps between the complicated UAV inflight icing phenomena under realistic, atmospheric icing conditions with turbulent ABL winds and the fundamental icing physics studies performed in laboratories with simplified assumptions and idealized lab settings. Quantitative field measurements to characterize inflight icing process and its detrimental effects on UAV flight performance under realistic, atmospheric icing conditions are very essential to fill the knowledge gaps to improve our understanding about the UAV icing phenomena for the development of more effective and robust anti−/de-icing strategies for UAV icing mitigation.

In the present study, we report a comprehensive flight-testing campaign to examine the characteristics of the inflight icing and its detrimental effects on the flight performance of a fixed-wing UAV. The fixed-wing UAV was hand launched and flew autonomously along a pre-planned flight trajectory under an atmospheric icing condition. A suite of advanced avionics and electronic sensors was installed onboard to monitor both the UAV flight status (e.g., flying speed, flight altitude, and power consumption of the propeller) and the environmental conditions (e.g., airspeed, ambient temperature, and relative humidity) along the pre-planned flight trajectory. A miniaturized digital camera was installed onboard to record the dynamic ice accretion and water runback process over the surface of the UAV wing during the flight. An advanced three-dimensional (3D) profile scanning system was also used to quantify the 3D shapes of the ice layers accreted on the UAV vertical stabilizer and propeller blades after the UAV finished the designated flight mission. The detrimental effects of the inflight icing on the UAV flying performance were evaluated quantitatively by comparing the measurement data collected during the flight mission with evident inflight icing against those under a normal, non-icing weather condition.

2. A brief description of the fixed-wing UAV used for the present study

In the present study, a fixed-wing UAV was used as the test platform for the flight test campaign to characterize the inflight icing process and to evaluate its effects on the UAV flight performance under a realistic, atmospheric icing condition. The fixed-wing UAV was developed "in-house" based on a commercially available airframe set (Skyhunter1800mm, Skynumber®,) along with an electric propeller and a

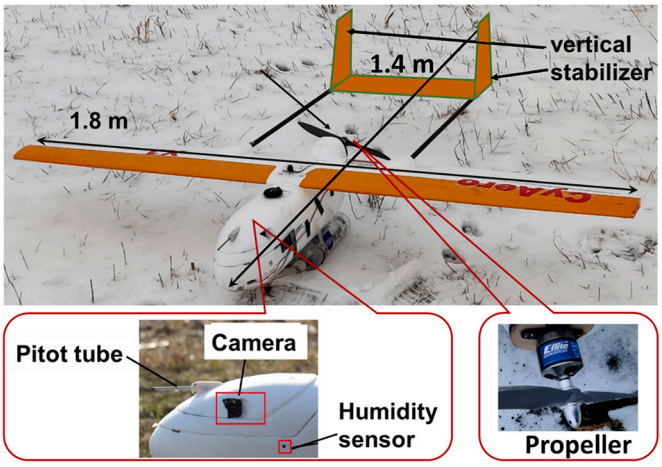

Fig. 1. The fixed-wing UAV used in the present study.

flight controller kit (Durandal, Holybro®). As shown schematically in Fig. 1, the airframe structures of the UAV (i.e., fuselage, wing, and vertical stabilizer) were made of light-weighted expanded polyolefin (EFO) foam enforced with carbon fibers. The UAV has a tip-to-tip wingspan of 1.8 m and nose-to-tail length of 1.4 m, which is sufficient to provide stable and long flight duration under different weather conditions. Table 1 summarizes the primary parameters of the fixed-wing UAV used in the present study.

As shown in Fig. 1, the UAV has a horizontal stabilizer which is composed of the left and right ailerons and associated elevators. It also has an H-tail design with two vertical stabilizers installed at the ends of the horizontal stabilizer. The H-tail design has been found to be very efficient to reduce the aircraft size, making the UAV being very convenient to transport while ensuring a good aerodynamic performance (Kurukularachchi et al., 2016). Since there is no rear fuselage, the H-tail design would also lead to a good flexibility in choosing propellers of different size for different flight missions. For the present study, the maximum takeoff weight of the UAV was set to be 3.5 kg, which is enough to carry all the avionics, sensors, batteries, and miniaturized digital cameras on board. A high-thrust brushless motor (Power 46, Eflite®) and a high-thrust propeller of 12 in. in diameter (APC12X7, APC®) were used to provide adequate thrust to ensure the stable flight of the UAV under different weather conditions.

A flight controller (Durandal, HolyBro®) with PX4 firmware was used as the flight control processor to navigate the UAV flying along a pre-planned flight trajectory. By programing the flight controller properly, the UAV can be operated in an autonomous flight mode to accomplish the flight missions along the same pre-planned flight trajectory under different weather conditions. A suite of avionics and electric sensors was installed onboard to monitor both the UAV flight status (e.g., the ground speed of the UAV, flight altitude, propeller power consumption, and UAV acceleration data) and the environmental conditions (e.g., airflow speed and direction, ambient temperature, relative humidity (RH) in the air). More specifically, a K-type thermocouple probe (K-type, Omega®) was used to measure the ambient temperature (i.e., static temperature) along the UAV flight trajectory. A pressure and humidity sensor (BME280, Bosch®) was also installed onboard to monitor the pressure and RH levels in the air during the flight. While the ground speed of the UAV was monitored by using an onboard GPS system to provide the UAV flight speed referred to the ground, a Pitot-static probe (MS4525DO) was installed at the nose of the UAV fuselage to measure the indicated airspeed (i.e., IAS). A miniaturized digital camera (Caddx Ratel 1200 TVL, CaddxFPV®) was also installed onboard to record the dynamic ice accretion process or/and water runback flows on the surface of the UAV wing when inflight icing occurs. While a Raspberry Pi unit (Raspberry Pi3, Raspberry®) was used as the core processor for the flight control and data acquisition of the onboard sensors, a pair of 900 MHz telemetry units (RFD9000, RFDesign®) were also installed onboard to provide a wireless connection between the flight controller and the ground station for "real-time" flight data transmission and UAV flight status monitoring. While the specifications of the onboard sensors are summarized in Table 2, further information about the avionics/sensors can be found in Siddique et al. (2022).

By installing a 4G-LTE connection unit onboard, the traceability of the UAV during the flight was secured through the wide coverage of the 4G/LTE technology. With the same 4G network, all the measurement data were broadcast to a Virtual Private Network (VPN) and associated terminals to minimize the risk of data loss or/and missing of the UAV during the flight campaign. Since the UAV was operated under a harsh environment with frozen cold temperature and high humidity during the flight mission with evident inflight icing, the cargo compartment of the UAV was insulated carefully to minimize the effects of the adverse weathers on the performances of the onboard avionics and sensors. Meanwhile, all the measurement data were backed up in "real time" to ensure the reliability of the quantitative measurements during the flight-testing campaign. It should also be noted that, while the UAV was operated in an autonomous flight mode for designed flight missions, it was also connected to a remote flight controller that can be used to control the UAV flight manually under emergency conditions. Fig. 2 summarizes schematically the avionics and electronic sensors installed onboard for the flight-testing campaign.

Table 1
The primary design parameters of the UAV used in the present study.

Specifications	Technical details
Wingspan	1800 mm
Length	1400 mm
Wing Area	0.36 m^2
Max Flying Weight	3.5 kg
Propeller	APC 12 × 7, APC®
Motor	Power 32, 770 KV, E-flite®

Table 2
Specifications of various onboard sensors.

Sensor type	Model Number	Accuracy
Thermocouple probe	K-type, Omega®	±1.0 °C
Atmospheric pressure/humidity sensor	BME280, BOSCH®	±0.25%
Pitot probe for airspeed measurement	MS4525DO, TE®	±0.25%

3. Measurement results and discussions

3.1. Flight-testing site and design of the UAV flight mission

The flight-testing campaign was performed at a designated UAV testing site on Iowa State University's BioCentury Research Farm (ISU-BCRF) where UAVs could take off and land over a vast farm field. Fig. 1 gives a snapshot image of the UAV at the flight-testing site before takeoff. As shown clearly in Fig. 1, the UAV was not equipped with a landing gear system due to the existence of a snow/ice layer on the ground. While the UAV was hand launched, the soft soil or snow/ice accumulated over the farmland would function as a cushion layer to mitigate the impact on the UAV during belly landings. It should be noted that, the UAV testing site is located at about 10 miles away from a small Municipal Airport at Boone, Iowa (i.e., KBNW airport), the weather data provided by the meteorological aerodrome report (METAR) system at KBNW airport was used as the reference for the preparation of the UAV flight-testing campaign.

Fig. 3(a) gives the aerial view of the designed UAV flight trajectory for the flight-testing campaign. The time evolution of the actual UAV flying altitude measured by using an onboard GPS system during one of the UAV flight missions was presented in Fig. 3(b). It can be seen clearly that each UAV flight mission would include five stages: takeoff, climbing, loitering, descending, and landing. For takeoff, the UAV was hand launched in the direction facing the surface wind with a full throttle for the propeller until a safe altitude was reached (i.e., at about 20 m above the ground). Then, the UAV would climb up rapidly until reaching a pre-planned loitering altitude (i.e., $H_{loitering}$) where inflight icing may take place based on the weather forecast of the nearby airport (i.e., KBNW airport). After reaching the loitering altitude (i.e., $H_{loitering} \approx 150$ m for the present study), the UAV would be flying around a pre-selected point in circles with a constant airspeed of $V_{airspeed.} \approx 16$ m/s and loitering duration of about 600 s. After finishing the loitering phase, the UAV would descend to a traffic-pattern altitude (i.e., at about 25 m above the ground) for the preparation of landing. Finally, the UAV would land on the ground in the direction facing the surface wind.

3.2. Selection of typical UAV flight missions to study inflight icing characteristics

The UAV flight-testing campaign was conducted over a period of 6

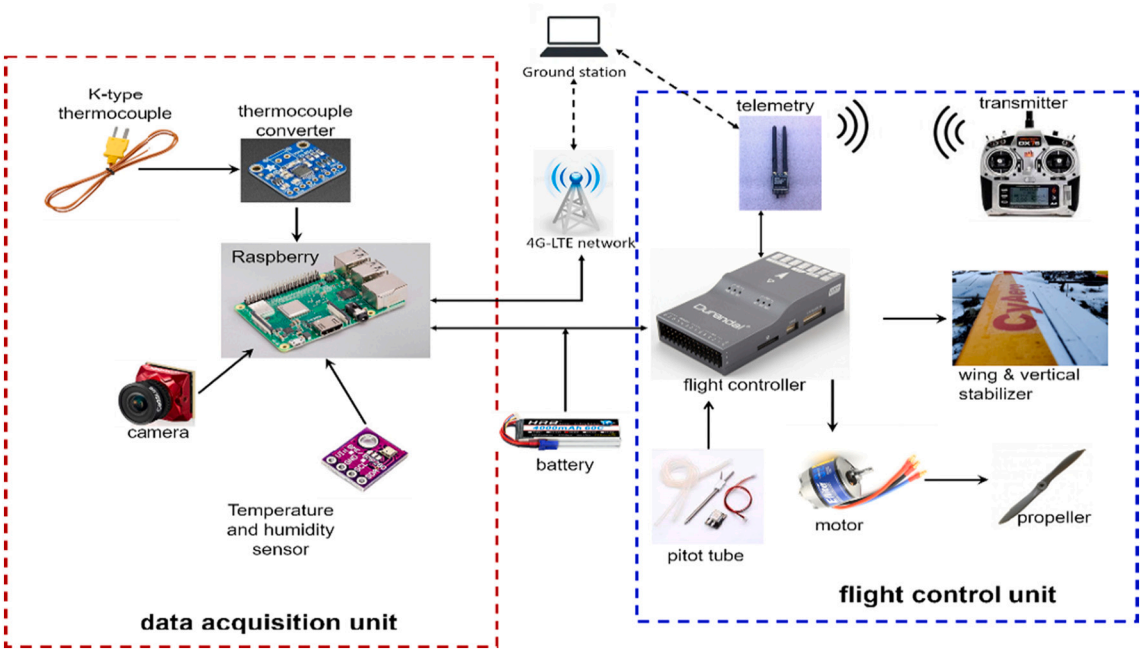

Fig. 2. A summary of the avionics and sensors installed onboard for the flight-testing campaign.

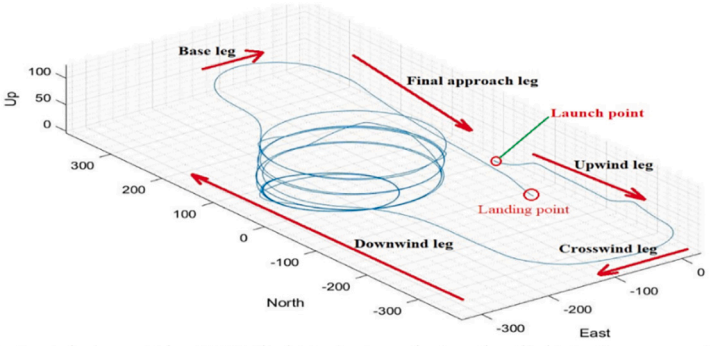

(a). Aerial view of the UAV flight trajectory during the flight-testing campaign

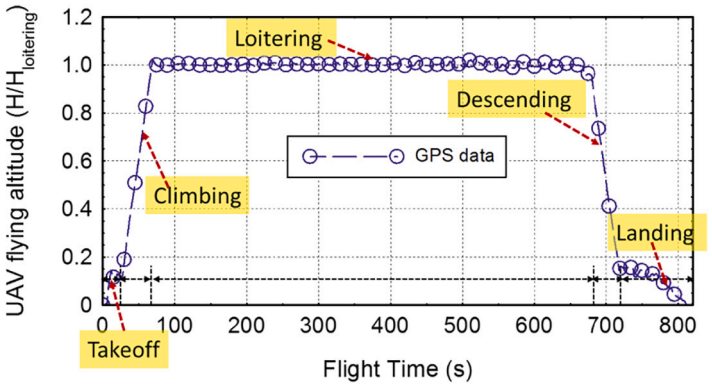

(b). UAV flying altitude measured by an onboard GPS system

Fig. 3. The measured flight trajectory during the UAV flight-testing campaign.

months, i.e., starting from September 2020 to March of 2021. It is well known that inflight icing phenomena would occur under certain specific weather conditions, which would require not only frozen cold ambient temperature (i.e., $T_{ambient} < 0.0$ °C), but also high liquid water content (LWC) or humidity levels in the air (Bernstein et al., 2000; Lamraoui et al., 2015; Veerakumar et al., 2020). While the ambient temperature at the flight-testing site located at Boone, Iowa is usually quite cold in winters, the air is dry with relatively low *LWC* and/or humidity levels in general. Among about 30 flight missions performed under the meteorological conditions for possible inflight icing, only 10 flight missions were found to have evident inflight icing with substantial ice layers accreted over the surfaces of UAV wings, fuselage, stabilizers, pitot

probe and propeller blades.

While over 50 flight missions were accomplished with the UAV flying autonomously along the same pre-planned flight trajectory under different weather conditions, two specific UAV flight missions were selected here for further analysis in the present study. The key meteorological parameters at the UAV flight site for the two selected UAV flight missions are summarized in Table 3 for comparison.

The flight mission #1 was accomplished on a warm and sunny day in the September of 2020 with the ambient temperature of $T_{ambient} \approx 20$ °C. Since the ambient temperature was well above the freezing temperature with a clear sky condition, no inflight icing was experienced by the UAV during the entire flight mission. Therefore, flight mission #1 was selected to represent a general case of UAV flight under a normal, non-icing weather condition.

The second flight mission (i.e., flight mission #2) was performed on a cold and cloudy day in March 2021, where the UAV was found to experience evident inflight icing. For the flight mission #2, while the ground temperature was found to be very close to the water freezing temperature (i.e., $T_{ambient} \approx 1.5$ °C), the air was quite wet with a high humidity level (i.e., RH > 80%). Meanwhile, the *overcast* cloud was reported to be at ~100 m above the ground, suggesting that the UAV would be loitering inside an overcast icing cloud.

Fig. 4 gives the profiles of the ambient temperature (i.e., static temperature) and RH values measured by the onboard sensors during flight mission #2. It can be seen clearly that the ambient temperature was found to decrease monotonically with the increasing altitude, as expected. While the *overcast* cloud was reported to be at about 100 m above the ground, the measured temperature data given in Fig. 4 confirmed that the *overcast* cloud was an icing cloud with its temperature being below the water freezing temperature. As the UAV climbed up to the loitering altitude of 150 m above the ground, the ambient temperature was found to be decreased down to $T_{ambient} \approx -1.6$ °C. Meanwhile, the measured relative humidity (RH) values given in Fig. 4 suggest that the overcast cloud was quite humid with the RH ≈ 87% at the UAV loitering altitude. As reported by Bian et al. (2014), a high RH value in the air would indicate a great LWC level in the cloud. Based on the meteorological report at KBNW airport, the overcast cloud was a cumulonimbus cloud. While typical LWC levels in cumulonimbus clouds are in the range of 1.0–3.0 g/m^3 (Linacre and Geerts, 1999), the size (i.e., MVD) of the airborne droplets in cumulus congestus would be ~20 μm (Kampe, 1950).

Since the weather conditions at the time when flight mission #2 was performed are very conducive to inflight icing, substantial ice structures were found to accrete over almost all the exposed UAV airframe surfaces (i.e., wings, fuselage, stabilizers, pitot probe and propeller blades) after the UAV finished the flight mission, which will be discussed in further detail later. It is worth noting that, since the ambient temperature near the ground was found to be still higher than the water freezing temperature for flight mission #2 as revealed quantitatively in Fig. 4, the ice accretion would not be able to take place during the takeoff and landing phases. Therefore, the inflight icing occurred only after entering the overcast cloud. The findings of the present study also highlight the dangerous scenarios if the design/planning of UAV flight missions is purely based on the meteorological data measured by the near ground equipment/instrumentations.

Table 3
Meteorological conditions of the two compared UAV flight missions.

Compared parameters	Flight mission #1 under a non-icing weather	Flight mission #2 with evident inflight icing
Temperature on the ground (°C)	20.00	1.50
Relative humidity on the ground (%)	35%	>80%
Wind speed on the ground (m/s)	5.6	6.7
Wind direction on the ground (°)	350.00	110.00
Sky condition	Clear	Overcast at ~100 m

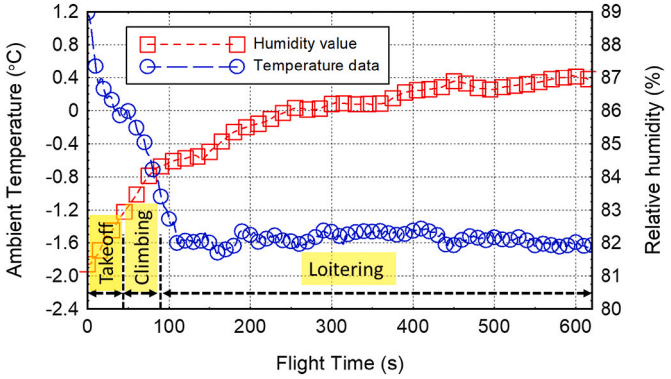

Fig. 4. Time evolution of the ambient temperature and relative humidity (RH) values measured by the onboard sensors during flight mission #2.

3.3. Characterization of the ice structures accreted over the UAV airframe surfaces

As indicated in Fig. 1, a miniaturized digital camera was installed onboard to record the dynamic icing process and water runback flows over the wing surface during the flight. Fig. 5(a) gives a typical snapshot image of the UAV wing acquired by using the onboard camera right after the UAV takeoff during flight mission #2 (i.e., referred as the "clean" wing without any ice accretion). The image of the same UAV wing acquired by the same digital camera at about 600 s later (i.e., referred as the "iced" wing due to the obvious ice accretion over the wing surface) was shown in Fig. 5(b). Since the weather conditions during flight mission #2 were relatively humid (i.e., with high RH and LWC values) and warm (i.e., $T_{ambient} > -2.0$ °C), the inflight icing process was expected to be a typical glaze icing process.

Based on the side-by-side comparison of the acquired images of the "clean" and "iced" UAV wing given in Fig. 5, general features of the inflight icing process over the UAV wing surface can be seen clearly. Instead of having a rather smooth leading edge and wing surface as revealed from the acquired image of the "clean" wing, the "iced" wing became much rougher with substantial ice structures accreted along the wing leading edge. In addition to forming transparent and glazy ice structures over the wing surface, obvious runback of unfrozen water was also observed, causing the formation of multiple water rivulets over the wing surface. The observed icing characteristics over the UAV wing surface confirmed that the inflight icing process during flight mission #2 was indeed a glaze icing process, as expected.

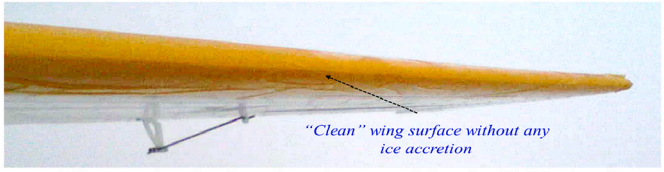

a). Image taken by the onboard camera right after UAV takeoff

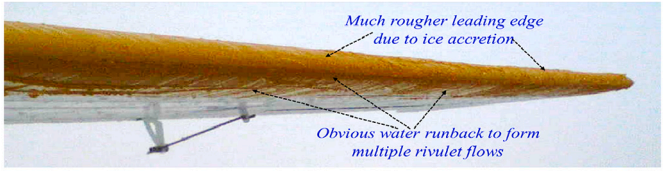

b). Image taken by the same onboard camera at 10 minutes later

Fig. 5. The acquired snapshot images of the UAV wing during flight mission #2.

More comprehensive investigations to characterize the ice structures accreted over the UAV airframe surfaces were performed after the UAV finished the flight mission and landed on the ground safely. At first, a set of images was taken immediately after the UAV landed on the ground. As shown clearly in Fig. 6, almost all the exposed airframe surfaces of the UAV were found to be covered with transparent ice layers. Substantial ice structures were found to accrete not only along the wing leading edge, but also over both the upper and lower surfaces of the UAV wing (Fig. 6a and b), due to the existence of obvious water runback over the wing surfaces. In addition to the wing surface, ice structures were also found to accrete on the surfaces of the UAV propeller, the fuselage, and the stabilizers (Fig. 6c, and d).

It should be noted that the ice accretion was found to block the pressure holes (i.e., both the ports for the total and static measurements) on the Pitot probe completely (Fig. 6e), leading to false readings of the measured airspeed, which will be discussed in the later section. For manned aircraft, the misreading of the airspeed from iced Pitot probes may directly threat the flight safety, leading to the loss of control over the aircraft. A number of deadly aircraft crashes was reported due to Pitot probe icing in recent years, including the catastrophic crash of Saratov Airlines Flight 703 killed all the 65 passages and 6 crew memebers on Febuary 02, 2018 (Jäckel et al., 2021). For the UAV used in the present study, an advanced flight control algorithm similar as that described in Lie and Gebre-Egziabher (2013) was adopted to make sure that the UAV control would not solely depend on Pitot probe reading. However, the misreading of the airspeed from the iced Pitot probe was still found to be a major hidden danger to the UAV flight safety.

After taking the images to record the ice accretion on the UAV airframe surfaces, the iced UAV propeller and one of the vertical stabilizers were preserved carefully in a portable freezer filled with dry ice and transported swiftly back to our research laboratory (i.e., within 30 min) for further characterization. A three-dimensional (3D) profile scanning system (Peng et al., 2020) was used in the present study to characterize the 3D shape of the ice layers accreted on the UAV propeller and the vertical stabilizer. The 3D profiler scanning system used in the present study is based on a novel digital-image-projection (DIP) technology with a structured light triangulation principle (Zhang et al., 2015). An optical projector was used to project a digital image with known characteristics onto the surface of the object of interest (i.e., the iced propeller blade and vertical stabilizer in the present study). Due to the ice accretion on the model surface, projected patterns would appear deformed when observed from any direction other than the projection axis. The 3D shapes of the iced model can be reconstructed via a comprehensive image processing procedure to calculate the displacement of the projected patterns in the acquired images of the iced model in related to the reference images without any ice accretion on the model surface. Further information about the technical basis and measurement procedure of the 3D profiler scanning system can be found in our recently published papers (Gao et al., 2019b; Peng et al., 2022; Zhang et al., 2015).

In the present study, the 3D shape scanning of the iced model was conducted inside a working freezing chamber with the iced propeller blade or vertical stabilizer being mounted on a rotating stage. Since the ice layer accreted over the iced propeller blade or vertical stabilizer was transparent, a thin layer of white powder was spray coated on the iced model by following the work of Gong and Bansmer (2015). After the test model was mounted properly on the rotation stage, it usually takes only about 30–60 s to finish the 3D profile scanning operation. Since the entire 3D scanning process of the iced models can be accomplished within 45 min after the UAV landed on the ground, the morphology changes of the accreted ice structures due to the 3D shape scanning operation are believed to be very small. It should also be noted that, the same system was also used by Veerakumar et al. (2020) to measure 3D printed hemispherical roughness elements on a test plate for the measurement accuracy estimation. Based on the measurements of about 500 points around a given hemispherical roughness element with a nominal height of 8.0 mm, the measurement uncertainty of the 3D profiler scanning system was found to be about 150 μm, i.e., ~ 2.0% of the targeted height of the measurements.

Fig. 7 shows the measurement result of the 3D scanning system to quantify the ice layer accreted on the UAV propeller blade. Since the UAV had a "rough" belly landing over the snow/ice covered farmland, the inevitable impact force during the UAV belly landing was found to cause a portion of the ice layer accreted over the outbound surface of the UAV propeller (i.e., in the region of $r/R > 0.46$) detached from the blade surface. While the 3D scanning results given in Fig. 7 can reflect only the remaining ice structures accreted on the blade surface, it is sufficient to reveal the significant profile changes of the propeller blade due to the ice accretion.

Based on the 3D scanning result, the outer profiles of the ice layer accreted on the UAV propeller were extracted. Fig. 7(c) gives the extracted outer profiles of the ice layer accreted on the UAV propeller at three selected spanwise sections, i.e., at $r/R \approx 0.32$, 0.46, and 0.60, respectively. It was revealed quantitatively that, while substantial ice structures were found to accrete along the leading edge of the propeller blade, the coverage of the accreted ice layer was found to extend to much further downstream locations, i.e., reaching almost the blade trailing edge due to the existence of obvious water runback over the

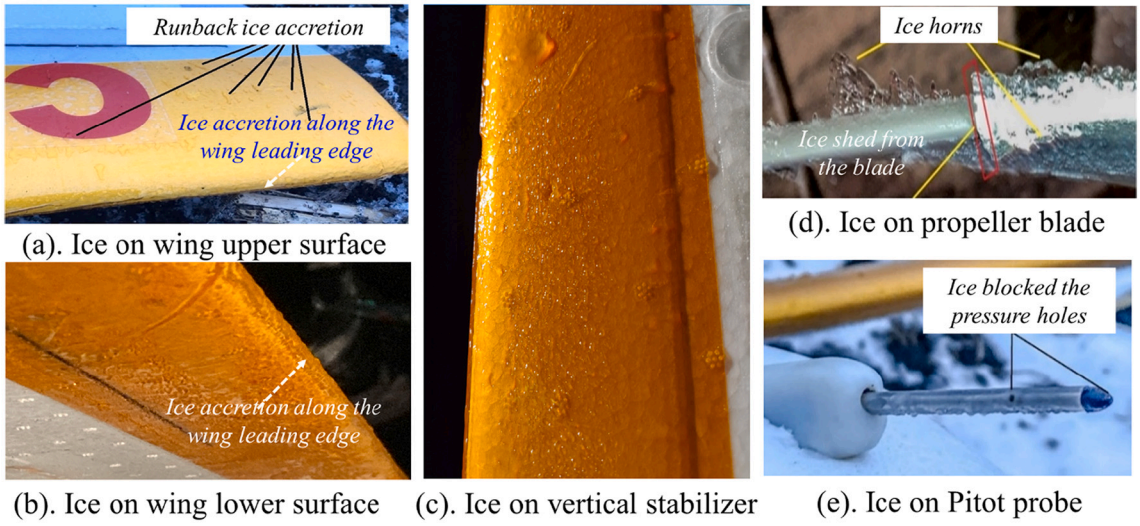

Fig. 6. Snapshot images of the ice structures accreted on the UAV airframe surface acquired right after the UAV landed on the ground.

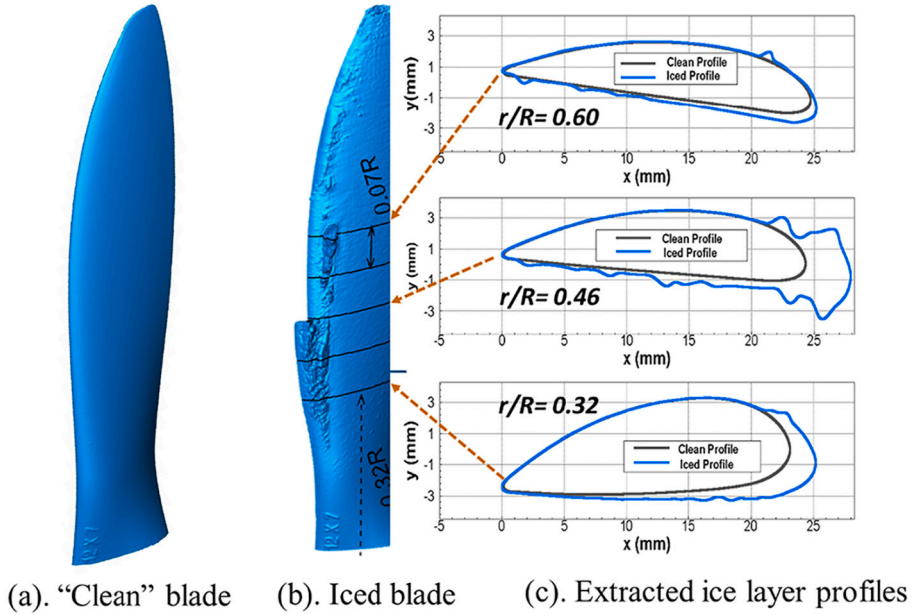

Fig. 7. Typical 3D scanning results of the "clean" and "iced" UAV propeller blade.

blade surface under the glaze icing condition of flight mission #2. In comparison to the smooth and streamlined airfoil surface of the "clean" blade, the iced blade was found to become much rougher due to the accretion of irregular-shaped ice structures over the blade surface. Similar as those reported in the previous studies (Karpen et al., 2022; Liu et al., 2018c; Müller and Hann, 2022), the devastation of the streamlined airfoil surface due to the ice accretion would degrade the aerodynamic performance of the UAV propeller significantly. It would result in a significant increase of the power consumption and dramatic decrease in the thrust generation for the iced UAV propeller, which were confirmed by the measured power consumption data to be discussed later. It should also be noted that the mass balance of the UAV propeller would be destroyed due to the randomly accreted ice over the blade surface. The rotation of the imbalanced propeller would provoke significant structural vibrations, causing great challenges to the UAV flight stability and imposing serious threats to the flight safety.

Fig. 8 gives the 3D scanning measurement results to reveal the characteristics of the ice accretion over the surface of the vertical stabilizer after flight mission #2. It can also be seen clearly that, while a portion of the ice structures accreted near the base of the vertical stabilizer was found to be shed off during the "rough" belly landing, substantial ice structures were still revealed to accumulate over the surface of the vertical stabilizer. The ice layer accumulated over the stabilizer surfaces would affect its aerodynamic performance greatly (Bragg et al., 1986), and consequently degrade the flight control performances of the stabilizer, posing a significant threat to the UAV flight stability.

It should also be noted that, while very similar characteristics of the ice accretion over airframe surfaces (e.g., airfoil/wing, propeller, and

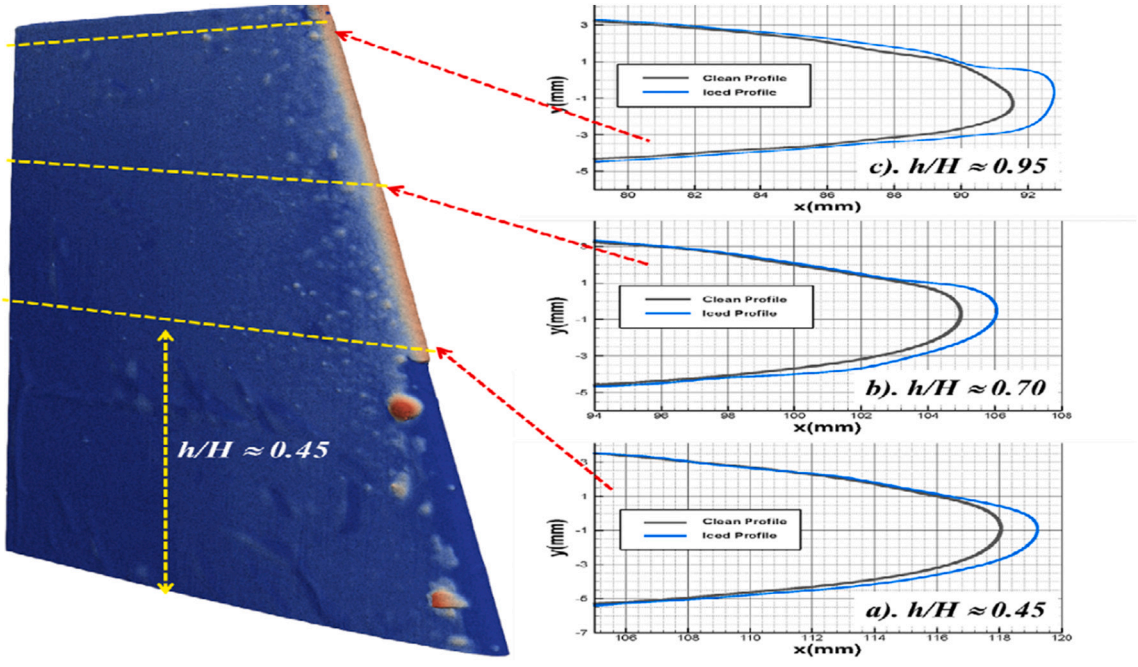

Fig. 8. 3D scanning results of the ice layers accreted on the UAV vertical stabilizer.

pitot probe) have been reported in previous studies by conducting icing tunnel experiments under idealized laboratory settings (Han et al., 2022b; Jäckel et al., 2021; Liu et al., 2018a; Liu et al., 2017), the measurement results reported here are believed to the first of its kind to reveal the ice accretion characteristics on UAV airframe surfaces after the UAV experienced an inflight icing event under a.

realistic, atmospheric icing condition. The quantitative field measurement data derived from the present study can be used not only to validate/verify the theoretical modelling and numerical simulations of UAV icing phenomena, but also to provide useful benchmarks to fill the knowledge gaps between the realistic UAV inflight icing phenomena and the fundamental icing physics studies performed in laboratories with simplified/idealized icing conditions.

3.4. *The detrimental effects of inflight icing on the UAV flight performance*

In the present study, the detrimental effects of the inflight icing on the UAV flight performance were also examined by analyzing the measurement results obtained during the flight mission with evident inflight icing (i.e., flight mission #2), in comparison to those under the non-icing weather condition (i.e., flight mission #1). Fig. 9 to Fig. 12 give side-by-side comparisons of the measured key parameters to quantify the UAV flight status as the UAV was set to fly along the same flight trajectory, but under different weather conditions.

As described above, the UAV was designed to fly with a constant flying speed of $V_{airspeed}$. ≈ 16 m/s during the flight mission. Fig. 9 gives the indicated airspeed (i.e., IAS) measured by using the onboard Pitot probe during the two compared flight campaigns. The measured IAS data represents the actual UAV flying speed in relation to the local airflow. For flight-testing campaign #1 (i.e., the non-icing case), the measured IAS values were always found to stay at the designated value during the entire flight mission, as expected. However, for flight-testing mission #2 with evident inflight icing, the measured IAS data were found to be at the designed value of $V_{airspeed}$. ≈ 16 m/s only at the beginning of the flight mission (i.e., $t < 180$ s). The IAS readings were found to decrease suddenly and even became a negative value at the later time (i.e., after the UAV loitering for about 80 s). The malfunction of the Pitot probe was found to be caused by the ice blockage of the pressure measuring holes, which was confirmed from the ice accretion image given in Fig. 6(e).

The sudden failure of the Pitot probe due to inflight icing was also found to cause a significant challenge to the UAV flight control system in maintaining a stable flight. With the airspeed reading from the Pitot probe dropped sharply, the pitch angle of the UAV was found to decrease suddenly, causing the UAV to lower its head and decrease its flight altitude abruptly. Since the advanced flight control algorithm similar as that described in Lie and Gebre-Egziabher (2013) was adopted for the UAV flight control in the present study, the UAV was still able to fly safely even though the Pitot probe was malfunctional due to the ice accretion. Since the UAV was designed to maintain a stable flight altitude and does not allow the sudden airspeed change, the throttle output of the UAV was found to increase rapidly (i.e., as revealed clearly from the measured power consumption data to be discussed later) to ensure the UAV returning to its designed flight altitude. In summary, despite the lack of a valid airspeed reading from the iced Pitot probe, the advanced flight control system was still able to ensure the UAV flying at the designated airspeed and flight altitude.

Fig. 10 gives the measured ground speed of the UAV from an onboard GPS system. Since the UAV was designed to be circling around a preselected point during the loitering phase as shown schematically in Fig. 3(a), the measured ground speed data given in Fig. 10 were found to vary periodically in the form of well-defined sinusoidal waves for both compared cases, due to the existence of substantial cross winds at the loitering altitude. The speeds of the cross winds at the loitering altitude, which can be estimated based on the fluctuating amplitude of the sinusoidal waves given in the measured ground speed plots (i.e., being about 8.0–10.0 m/s), were found to be very comparable for the two compared cases.

Fig. 11 gives the measured power consumption data of the UAV propeller during the two compared flight missions, which can be used to reveal the detrimental effects of inflight icing on the UAV flight performance more clearly and quantitatively. It can be seen clearly that the UAV was found to have relatively high-power consumption levels at the takeoff and climbing stage since the extra power was needed by the propeller to accelerate the UAV and to increase its flying altitude. After reaching the loitering altitude, while the UAV was set to be circling around at the same altitude with a constant airspeed (i.e., having the same IAS value of 16 m/s), the power consumption level of the UAV propeller was found to reduce substantially. For flight mission #1 without inflight icing, the instantaneous power consumption of the UAV propeller was found to fluctuate randomly during the loitering flight, which is believed to be closely related to the turbulent nature of the surface winds at the loitering altitude. The moving-averaged values (i.e., the ensemble-averaged value within each 5 s) of the power consumption data during the entire loitering phase were found to stay almost at a constant value of $P_{averaged} \approx 250$ W (i.e., from $t = 70$ s to $t = 630$ s). Based on the measurement results of the flight campaigns on different days, the averaged power consumption of the UAV during loitering phase was found to vary within 10% under the weather conditions without inflight icing.

However, for flight mission #2, ice would start to accrete over every exposed airframe surface and rotating propeller blade as soon as the UAV flew into the icing cloud (i.e., starting at $t \approx 50$ s). Substantial ice structures would have already accreted on the airframe surfaces as the UAV climbed to the loitering altitude at the time of $t \approx 90$ s. The ice accretion over the UAV airframe surfaces would degrade the UAV aerodynamic performance significantly by increasing drag, while

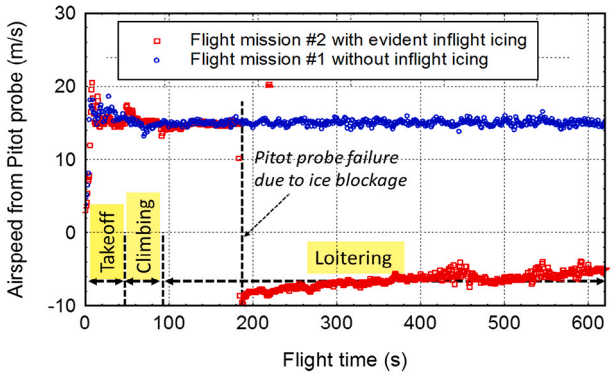

Fig. 9. The measured IAS data during the two compared flight missions.

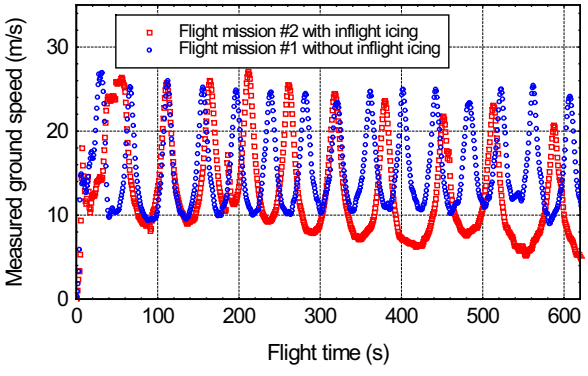

Fig. 10. Comparison of the measured GS value of the UAV during the two flight missions.

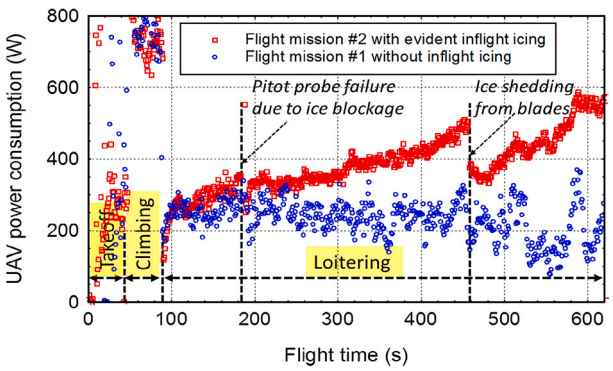

Fig. 11. Comparison of the measured power consumption of the UAV propeller during the two flight missions.

decreasing lift. As a result, in comparison to the scenario with the UAV flying under a normal, non-icing weather condition (i.e., flight mission #1), the UAV propeller would require extra power inputs to generate extra thrust to overcome the larger drag force acting on the iced UAV. Meanwhile, similar as that reported in Liu et al. (2019), the ice accretion on the rotating propeller blade would degrade its thrust generation capacity greatly while increasing the power consumption substantially. All these would contribute to a greater power consumption of the UAV propeller during flight mission #2. Therefore, the UAV was found to have about ~20% greater power consumption at the beginning of the loitering flight for flight mission #2 (i.e., $P_{averaged} \approx 280$ W at the time of $t \approx 100$ s), in comparison to that of flight mission #1.

With the UAV flying inside the icing cloud during the loitering phase of flight mission #2, the ice layers accreted over the UAV airframe surfaces and the propeller blade would become thicker and thicker as the flight time increases. Thus, the power consumption values of the UAV propeller were found to increase continuously, until experiencing an abrupt drop at the time of $t \approx 460$ s (i.e., the ensemble-averaged power consumption value increased from $P_{averaged} \approx 280$ W at the beginning of the loiter phase to a much higher level of $P_{averaged} \approx 500$ W at $t \approx 460$ s).

It should be noted that, with the ice layer accreted on the rotating propeller blade becoming thicker and thicker, the centrifugal forces acting on the ice structures would also increase rapidly. As the accreted ice mass becomes big enough, the associated centrifugal force would become greater than the ice adhesion forces over the blade surface. Similar as that described in Papadakis et al. (2009) and Nilamdeen et al. (2019), the strong centrifugal force would cause a portion of the accreted ice to detach from the rotating propeller blade. The abrupt ice shedding would cause a rapid recovery of the propeller performance (i.e., a greater thrust generation and lower power consumption), causing the sudden drop of the measured power consumption data at the time of $t \approx 460$ s (i.e., the ensemble-averaged power consumption decreased suddenly from $P_{averaged} \approx 500$ W to $P_{averaged} \approx 360$ W). Since the UAV was still flying in the icing cloud, the ice accretion process would re-start again over the rotating blade surface. As a result, the measured power consumption value of the UAV propeller was found to increase rapidly from $P_{averaged} \approx 360$ W to $P_{averaged} \approx 560$ within a short duration of 140 s, as revealed in Fig. 11.

In the present study, the averaged power consumption of the UAV propeller during the entire loitering flight phase was calculated to indicate the detrimental effects of the inflight icing on the UAV power consumption quantitatively. It was found that, while the averaged power consumption level of the UAV in the loitering flight was about $P_{loitering} \approx 240$ W under a normal, non-icing weather condition (i.e., during flight mission #1), the corresponding value was found to be increased to $P_{loitering} \approx 450$ W as the UAV was flying inside the overcast icing cloud (i.e., during flight mission #2). In summary, with the same UAV flying at the same loitering altitude for the same loitering duration, the UAV would consume about 80% more power when flying under the icing condition (i.e., flight mission #2) than the case under a normal, non-icing weather condition (i.e., flight mission #1). It should be noted that the significant increase in the UAV power consumption due to inflight icing would cause great challenges to the UAV flight due to the limited power source available to the UAV, which would reduce the UAV flight time and/or shorten their flight distance, thereby, imposing great challenges to the UAV flight safety.

In addition to causing extra power consumption to the UAV propeller, inflight icing and abruptic ice shedding from the rotating propeller blade were also found to provoke greater structural vibrations, which can also impose greater challenges to the UAV flight stability. In the present study, the UAV was also equipped with an accelerometer onboard, which can be used to quantify the vibration characteristics of the UAV flying under different weather conditions. Fig. 12 gives typical outputs of the onboard accelerometer during the two compared flight missions. It should be noted that the onboard accelerator can measure structural vibrations of the UAV in all three directions. Since very similar features were revealed from all three components of the measured accelerator data, only the Z-component values of the measured acceleration vectors (i.e., a_z, along the vertical direction) were analyzed here for conciseness.

As revealed clearly in Fig. 12, with the UAV flying under a normal, non-icing weather condition (i.e., flight mission #1), the vibration amplitudes of the UAV were found to be almost unchanged during the entire flight mission, which were closely related to the turbulence intensity or/and gust level of the surface winds during the flight campaign.

As for the UAV flying under the atmospheric icing condition (i.e., flight mission #2), the vibration amplitudes of the UAV were found to become much greater. The greater vibrations for the UAV flying under the icing condition are believed to be caused by the detrimental effects of the ice accretion on the UAV airframe surface and the rotating propeller blade. Similar as those reported in the previous studies (Han et al., 2022b; Liu et al., 2019), ice accretion on the propeller blade surface would dramatically change the outer profiles of the propeller blade, which would induce large-scale airflow separation over the blade surface, thereby, inducing unsteady aerodynamic loads acting on the propeller to excite the structural vibrations. Furthermore, the rotation of the imbalanced propeller due to the uneven ice coverage over the propeller blade as those shown in Fig. 7 would also impose extra unsteady loads to the propeller to cause greater vibrations.

It can also be seen that, as the flight time increases, corresponding to more and more ice structures accreted on the propeller blades, the vibration amplitude of the UAV was found to increase monotonically until the accreted ice structures were shed abruptly from the rotating propeller blade. As shown clearly in Fig. 12, after the accreted ice was shed away from the surface of the rotating propeller blades at $t \approx 460$ s, the fluctuation amplitudes of the UAV were found to be decreased greatly,

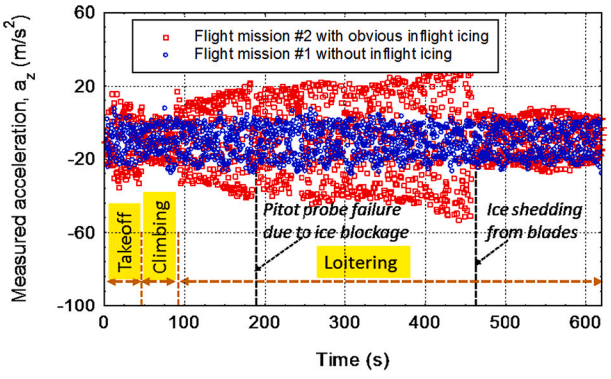

Fig. 12. Comparison of the measured acceleration data during the two flight missions.

as expected.

4. Conclusions

A flight-testing campaign was conducted to examine the characteristics of the inflight icing and its effects on the flight performance of a fixed-wing Unmanned-Aerial-Vehicle (UAV). While the UAV was deployed to fly autonomously along a pre-planned flight trajectory under a realistic, atmospheric icing condition, various advanced avionics and electronic sensors were installed onboard to monitor both the UAV flight status (e.g., flying speed, flight altitude, and power consumption) and the environmental conditions (e.g., airspeed, ambient temperature, and relative humidity). In addition to using a miniaturized, onboard camera to record the dynamic icing process and transient water runback flows on the UAV wing surface during the flight, the shape of the ice layers accreted on the UAV vertical stabilizer and propeller blade were also characterized by using a three-dimensional (3D) profile scanning system after the UAV finished the flight mission and landed on the ground. The detrimental effects of the inflight icing on the UAV flying performance were evaluated quantitatively based on a side-by-side comparison of the measurement data obtained during the flight mission with evident inflight icing against those with the UAV flying along the same flight trajectory under a normal, non-icing weather condition.

Substantial ice structures were found to accrete over nearly all the exposed airframe surfaces (i.e., UAV wings, fuselage, stabilizers, Pitot probe and propeller) after the UAV finished the flight mission with evident inflight icing. In addition to having obvious ice accretion along the leading edges of the wings and stabilizers, considerable ice structures were also found to accumulate over both the pressure-side and suction-side surfaces of the UAV wings and stabilizers. Noticeable water runback flows were observed over the wing/stabilizer surfaces during the flight. The ice layer accreted over the surface of the Pitot probe was found to cause a complete blockage of the pressure holes, leading to false airspeed readings from the iced Pitot probe, which imposed serious threats the UAV flight safety.

The ice structures accreted on the propeller blade were found to degrade the perfomance of the UAV propeller signficantly. In comparison to the case with the UAV flying under a normal, non-icing weather condition, the iced propeller was found to comsume over 80% more power to accomplish the same flight mission. Furthermore, the mass imbalance of the rotating propeller caused by random ice accretion over the blade was found to impose extra loads to the propeller, provoking much greater structural vibrations to the UAV. The detaching/shedding of large ice chunks from the rotating propeller blade was also found to cause an abruptic increase of the structural vibrations, imposing significant threats to the UAV stability and flight safety.

It should be noted, while extensive studies have been conducted in recent years to study UAV icing phenomena and to evaluate the UAV performance degradation induced by the ice accretion by performing icing tunnel experiments with simplified laboratory settings, the work reported here is believed to be the first comprehensive flight-testing campaign to examine the characteristics of the ice accretion over the airframe surfaces of a fixed-wing UAV and to evaluate the effects of the inflight icing on the flight performance with the UAV flying under a realistic, atmospheric icing condition. The quantitative field measurement data of the present study can be used not only to validate/verify the theoretical modelling and numerical simulations of UAV icing phenomena, but also to provide useful benchmarks to fill the knowledge gaps between the realistic UAV inflight icing phenomena and the fundamental icing physics studies performed in laboratories with simplified/idealized icing conditions. The new findings derived from the present studies would lead to a better understanding of the UAV inflight icing process, which is essential for the development of effective and robust anti−/de-icing strategies to ensure safer and more efficient operation of UAVs in cold weather. It should also be noted that the research work reported here is a portion of a more comprehensive research program to characterize the effects of typical adverse weathers (e.g., wind gusts, rain, snow, and icing) and develop novel mitigation strategies for assured UAV flight safety in all-weather conditions. While the research is still ongoing, more research findings will be reported in the future as the research progresses.

Authors' statements

We confirm that the manuscript has been read and approved by all named authors and that there are no other persons who satisfied the criteria for authorship but are not listed.

We further confirm that the order the authors listed in the manuscript has been approved by all of us. We also confirm that we have given due consideration to the protection of intellectual property associated with this work and that there are no impediments to publication, including the timing of publication, with respect to intellectual property.

We understand that the Corresponding Author is the sole contact for the Editorial process (including Editorial Manager and direct communications with the office). He/she is responsible for communicating with the other authors about progress, submissions of revisions and final approval of proofs.

We confirm that we have provided a current, correct email address which is accessible by the Corresponding Author, and which has been configured to accept email from.

Declaration of Competing Interest

The authors declare that they have no known competing financial interests or personal relationships that could have appeared to influence the work reported in this paper.

Data availability

The acquired images of ice accretion over the UAV airframe surfaces, measured 3D shapes of the ice layers accreted over the surfaces of the UAV vertical stabilizer and propeller blade, propeller power consumption and structural vibration data are included in the article. All the measurement results obtained during the UAV flight-testing campaign have been deposited at the website of the Aircraft Icing Physics and Anti-/De-Icing Technology Laboratory of Iowa State University (https://www.aere.iastate.edu/icing/), which will be available to general public per NSF data share guidelines.

Acknowledgments

The research work is partially supported by the National Science Foundation (NSF) of the USA under award numbers CBET-1916380 and CBET-1935363 and Iowa Energy Center for Wind Turbine Icing Study under the IEC Competitive Grant No. 312350.

References

Aggarwal, S., Schnabel, W., Buist, I., Garron, J., Bullock, R., Perkins, R., Potter, S., Cooper, D., 2017. Aerial application of herding agents to advance in-situ burning for oil spill response in the Arctic: a pilot study. Cold Reg. Sci. Technol. 135, 97–104. https://doi.org/10.1016/J.COLDREGIONS.2016.12.010.

Armanini, S.F., Polak, M., Gautrey, J.E., Lucas, A., Whidborne, J.F., 2016. Decision-making for unmanned aerial vehicle operation in icing conditions. CEAS Aeronaut. J. 7, 663–675. https://doi.org/10.1007/s13272-016-0215-2.

Bernstein, B.C., Ratvasky, T.P., Miller, D.R., McDonough, F., 2000. Freezing rain as an In-Flight Icing Hazard. NASA Report TM-2000-210058.

Bian, Y.X., Zhao, C.S., Ma, N., Chen, J., Xu, W.Y., 2014. A study of aerosol liquid water content based on hygroscopicity measurements at high relative humidity in the North China Plain. Atmos. Chem. Phys. 14, 6417–6426. https://doi.org/10.5194/acp-14-6417-2014.

Bie, D., Li, D., Xiang, J., Li, H., Kan, Z., Sun, Y., 2021. Design, aerodynamic analysis and test flight of a bat-inspired tailless flapping wing unmanned aerial vehicle. Aerosp. Sci. Technol. 112 https://doi.org/10.1016/j.ast.2021.106557.

Bottyán, Z., 2014. In-flight icing characteristics of unmanned aerial vehicles during special atmospheric condition over the carpathian-basin. ACTA Geogr. Debrecina Landsc. Environ. 7, 74–80.
Bragg, M.B., Gregorek, G.M., Lee, J.D., 1986. Airfoil Aerodynamics in Icing Conditions. J. Aircr. 23 https://doi.org/10.2514/3.45269.
Cao, Y., Tan, W., Wu, Z., 2018. Aircraft icing: an ongoing threat to aviation safety. Aerosp. Sci. Technol. 75, 353–385. https://doi.org/10.1016/j.ast.2017.12.028.
Eckerstorfer, M., Bühler, Y., Frauenfelder, R., Malnes, E., 2016. Remote sensing of snow avalanches: recent advances, potential, and limitations. Cold Reg. Sci. Technol. 121, 126–140. https://doi.org/10.1016/J.COLDREGIONS.2015.11.001.
Gao, L., Liu, Y., Hu, H., 2019a. An experimental investigation of dynamic ice accretion process on a wind turbine airfoil model considering various icing conditions. Int. J. Heat Mass Transf. 133, 930–939. https://doi.org/10.1016/J.IJHEATMASSTRANSFER.2018.12.181.
Gao, L., Veerakumar, R., Liu, Y., Hu, H., 2019b. Quantification of the 3D shapes of the ice structures accreted on a wind turbine airfoil model. J. Vis. 22, 661–667. https://doi.org/10.1007/s12650-019-00567-4.
Gong, X., Bansmer, S., 2015. Laser scanning applied for ice shape measurements. Cold Reg. Sci. Technol. 115, 64–76. https://doi.org/10.1016/J.COLDREGIONS.2015.03.010.
Han, N., Hu, Haiyang, Hu, Hui, 2022a. An Experimental Investigation to Assess the Effectiveness of Various Anti-Icing Coatings for UAV Propeller Icing Mitigation. AIAA Aviat. 2022 Forum. https://doi.org/10.2514/6.2022–3964.
Han, N., Hu, Haiyang, Hu, Hui, 2022b. An Experimental Investigation on the Dynamic Ice Accretion Process over the Blade Surface of a Rotating UAV Propeller. In: AIAA Science and Technology Forum and Exposition, AIAA SciTech Forum, pp. 151–170. https://doi.org/10.2514/6.2022-1538.
Hann, R., 2019. Uav icing: Comparison of lewice and fensap-ice for anti-icing loads. In: AIAA Scitech 2019 Forum. https://doi.org/10.2514/6.2019-1286.
Hann, R., Johansen, T.A., 2020. Unsettled topics in unmanned aerial vehicle icing. In: SAE Edge Report, pp. 3–22. https://doi.org/10.4271/EPR2020008.
Hann, R., Johansen, T.A., 2021. UAV icing: the influence of airspeed and chord length on performance degradation. Aircr. Eng. Aerosp. Technol. 93, 832–841. https://doi.org/10.1108/AEAT-06-2020-0127/FULL/HTML.
Hann, R., Wenz, A., Gryte, K., Johansen, T.A., 2017. Impact of atmospheric icing on UAV aerodynamic performance. In: 2017 Work. Res. Educ. Dev. Unmanned Aer. Syst. RED-UAS 2017, pp. 66–71. https://doi.org/10.1109/RED-UAS.2017.8101645.
Hann, R., Hearst, R.J., Sætran, L.R., Bracchi, T., 2020. Experimental and numerical icing penalties of an S826 airfoil at low reynolds numbers. Aerosp 7. https://doi.org/10.3390/AEROSPACE7040046. Page 46 7, 46.
Hawley, R.L., Millstein, J.D., 2019. Quantifying snow drift on Arctic structures: a case study at Summit, Greenland, using UAV-based structure-from-motion photogrammetry. Cold Reg. Sci. Technol. 157, 163–170. https://doi.org/10.1016/J.COLDREGIONS.2018.10.007.
Hu, Q., Xu, X., Leng, D., Shu, L., Jiang, X., Virk, M., Yin, P., 2021. A method for measuring ice thickness of wind turbine blades based on edge detection. Cold Reg. Sci. Technol. 192, 103398 https://doi.org/10.1016/J.COLDREGIONS.2021.103398.
Ignatyev, D.I., Khrabrov, A.N., Kortukova, A.I., Alieva, D.A., Sidoryuk, M.E., Bazhenov, S.G., 2020. Interplay of unsteady aerodynamics and flight dynamics of transport aircraft in icing conditions. Aerosp. Sci. Technol. 104, 105914 https://doi.org/10.1016/j.ast.2020.105914.
Jäckel, R., Gutiérrez-Urueta, G., Tapia, F., 2021. A review on Pitot tube icing in aeronautics: Research- design and characterization – future trends. Flow Meas. Instrum. 81, 102033 https://doi.org/10.1016/J.FLOWMEASINST.2021.102033.
Kampe, A.H.J., 1950. Visibility and liquid water conent in the free atmosphere. J. Meteorol. 7, 166. https://doi.org/10.1175/1520-0469(1950)007<0054:VALWCI>2.0.CO;2.
Karpen, N., Diebald, S., Dezitter, F., Bonaccurso, E., 2022. Propeller-integrated airfoil heater system for small multirotor drones in icing environments: Anti-icing feasibility study. Cold Reg. Sci. Technol. 201, 103616 https://doi.org/10.1016/J.COLDREGIONS.2022.103616.
Kurukularachchi, P.L., Munasinghe, S.R., De Silva, H.R.P.S., 2016. Stability analysis for a twin boom H- tail Medium Scale UAV through simulated dynamic model. In: 2nd Int. Moratuwa Eng. Res. Conf. MERCon 2016, pp. 415–420. https://doi.org/10.1109/MERCON.2016.7480177.
Lamraoui, F., Fortin, G., Perron, J., Benoit, R., 2015. Canadian icing envelopes near the surface and its impact on wind energy assessment. Cold Reg. Sci. Technol. 120, 76–88. https://doi.org/10.1016/j.coldregions.2015.09.007.
Li, L., Liu, Y., Zhang, Z., Hu, H., 2019. Effects of thermal conductivity of airframe substrate on the dynamic ice accretion process pertinent to UAS inflight icing phenomena. Int. J. Heat Mass Transf. 131, 1184–1195. https://doi.org/10.1016/J.IJHEATMASSTRANSFER.2018.11.132.
Lie, F.A.P., Gebre-Egziabher, D., 2013. Synthetic air data system. Jorunal Aircr. 50, 1234–1249. https://doi.org/10.2514/1.C032177.
Linacre, E., Geerts, B., 1999. Cloud Liquid Water Content, Drop Sizes, and Number of Droplets [WWW Document]. URL. http://www-das.uwyo.edu/~geerts/cwx/notes/chap08/moist_cloud.html (accessed 12.4.22).
Liu, Y., Hu, H., 2018. An experimental investigation on the unsteady heat transfer process over an ice accreting airfoil surface. Int. J. Heat Mass Transf. 122, 707–718.
Liu, Y., Li, L., Ning, Z., Tian, W., Hu, H., 2017. An experimental study on the transient ice accretion process over the blade surfaces of a rotating UAS propeller. In: AIAA SciTech Forum - 55th AIAA Aerospace Sciences Meeting, pp. 1–18. https://doi.org/10.2514/6.2017–0727.
Liu, Y., Li, L., Li, H., Hu, H., 2018a. An experimental study of surface wettability effects on dynamic ice accretion process over an UAS propeller model. Aerosp. Sci. Technol. 73, 164–172. https://doi.org/10.1016/j.ast.2017.12.003.
Liu, Y., Li, L., Ning, Z., Tian, W., Hu, H., 2018b. Experimental investigation on the dynamic icing process over a rotating propeller model. J. Propuls. Power 0, 1–15. https://doi.org/10.2514/1.B36748.
Liu, Y., Li, L., Ning, Z., Tian, W., Hu, H., 2018c. Experimental investigation on the dynamic icing process over a rotating propeller model. J. Propuls. Power 34, 933–946. https://doi.org/10.2514/1.B36748.
Liu, Y., Li, L., Chen, W., Tian, W., Hu, H., 2019. An experimental study on the aerodynamic performance degradation of a UAS propeller model induced by ice accretion process. Exp. Thermal Fluid Sci. 102, 101–112. https://doi.org/10.1016/j.expthermflusci.2018.11.008.
Müller, N.C., Hann, R., 2022. UAV icing: a performance model for a UAV propeller in icing conditions. In: AIAA Aviat. 2022 Forum. https://doi.org/10.2514/6.2022-3903.
Nilamdeen, S., Zhang, Y., Ozcer, I., Baruzzi, G.S., 2019. An ice shedding model for rotating components. In: SAE Tech. Pap. 2019-June. https://doi.org/10.4271/2019-01-2003.
Oo, N.L., Richards, P.J., Sharma, R.N., 2020. Ice-induced separation bubble on RG-15 airfoil at low Reynolds number. AIAA J. 58, 5156–5167. https://doi.org/10.2514/1.J059257.
Oswald, J.W., Enache, A., Hann, R., Glabeke, G., Lutz, T., 2022. UAV Icing: Experimental and Numerical Study of Glaze Ice Performance Penalties on an RG-15 Airfoil. AIAA Sci. Technol. Forum Expo. AIAA SciTech Forum 2022. https://doi.org/10.2514/6.2022-1976.
Pajares, G., 2015. Overview and current status of remote sensing applications based on unmanned aerial vehicles (UAVs). Photogramm. Eng. Remote. Sens. 81, 281–329. https://doi.org/10.14358/PERS.81.4.281.
Papadakis, M., Yeong, H.W., Shimoi, K., Wong, S.H., 2009. Ice shedding experiments with simulated ice shapes. In: 1st AIAA Atmos. Sp. Environ. Conf. https://doi.org/10.2514/6.2009-3972.
Peng, Y., Veerakumar, R., Liu, Y., He, X., Hu, H., 2020. An experimental study on dynamic ice accretion and its effects on the aerodynamic characteristics of stay cables with and without helical fillets. J. Wind Eng. Ind. Aerodyn. 205, 104326 https://doi.org/10.1016/j.jweia.2020.104326.
Peng, Y., Veerakumar, R., Zhang, Z., Hu, Haiyang, Liu, Y., He, X., Hu, Hui, 2022. An experimental study on mitigating dynamic ice accretion process on bridge cables with a superhydrophobic coating. Exp. Thermal Fluid Sci. 132, 110573 https://doi.org/10.1016/J.EXPTHERMFLUSCI.2021.110573.
Politovich, M.K., 2000. Predicting Glaze or Rime Ice Growth on Airfoils. J. Aircr. 37, 117–121. https://doi.org/10.2514/2.2570.
Revuelto, J., Alonso-Gonzalez, E., Vidaller-Gayan, I., Lacroix, E., Izagirre, E., Rodríguez-López, G., López-Moreno, J.I., 2021. Intercomparison of UAV platforms for mapping snow depth distribution in complex alpine terrain. Cold Reg. Sci. Technol. 190, 103344 https://doi.org/10.1016/J.COLDREGIONS.2021.103344.
Siddique, M.A., Han, N., Hu, H., 2022. Development of an experimental unmanned-aerial-system (UAS) to study the effects of adverse weathers on its flight performance. In: AIAA Sci. Technol. Forum Expo. AIAA SciTech Forum 2022. https://doi.org/10.2514/6.2022-1646.
Siquig, R.A., 1990. Impact of Icing on Unmanned Aerial Vehicle (UAV) Operations, DTIC Report. https://apps.dtic.mil/sti/citations/ADA231191.
Sørensen, K.L., Helland, A.S., Johansen, T.A., 2015. Carbon nanomaterial-based wing temperature control system for in-flight anti-icing and de-icing of unmanned aerial vehicles. In: 2015 IEEE Aerospace Conference, pp. 1–6.
Szilder, K., McIlwain, S., 2012. In-flight icing of UAVs – the influence of flight speed coupled with chord size. Can. Aeronaut. Sp. J. 58, 83–94. https://doi.org/10.5589/q12-007.
Szilder, K., Yuan, W., 2017. In-flight icing on unmanned aerial vehicle and its aerodynamic penalties. Prog. Flight Phys. 9, 173–188. https://doi.org/10.1051/eucass/2016090173.
Tsouros, D.C., Bibi, S., Sarigiannidis, P.G., 2019. A review on UAV-based applications for precision agriculture. Information 10, 349. https://doi.org/10.3390/info10110349.
Veerakumar, R., Gao, L., Liu, Y., Hu, H., 2020. Dynamic ice accretion process and its effects on the aerodynamic drag characteristics of a power transmission cable model. Cold Reg. Sci. Technol. 169, 102908 https://doi.org/10.1016/j.coldregions.2019.102908.
Vercillo, V., Karpen, N., Laroche, A., Mayén Guillén, J.A., Tonnicchia, S., de Andrade Jorge, R., Bonaccurso, E., 2019. Analysis and modelling of icing of air intake protection grids of aircraft engines. Cold Reg. Sci. Technol. 160, 265–272. https://doi.org/10.1016/J.COLDREGIONS.2019.01.012.
Waldman, R.M., Hu, H., 2016. High-speed imaging to quantify transient ice accretion process over an airfoil. J. Aircr. 53, 369–377. https://doi.org/10.2514/1.C033367.
Winter, A., Hann, R., Wenz, A., Gryte, K., Johansen, T.A., 2019. Stability of a flying wing UAV in icing conditions. In: 8th Eur. Conf. Aeronaut. Aerosp. Sci. (EUCASS). https://doi.org/10.13009/EUCASS2019-906.
Yan, S., Opazo, T.I., Langelaan, J.W., Palacios, J.L., 2020. Experimental evaluation and flight simulation of coaxial-rotor vehicles in icing clouds. J. Am. Helicopter Soc. 65 https://doi.org/10.4050/JAHS.65.022011.
Zhang, B., Tang, L., Roemer, M., 2014. Probabilistic weather forecasting analysis for unmanned aerial vehicle path planning. J. Guid. Control. Dyn. 37, 309–312. https://doi.org/10.2514/1.61651.
Zhang, K., Tian, W., Hu, H., 2015. An experimental investigation on the surface water transport process over an airfoil by using a digital image projection technique. Exp. Fluids 56, 173. https://doi.org/10.1007/s00348-015-2046-z.